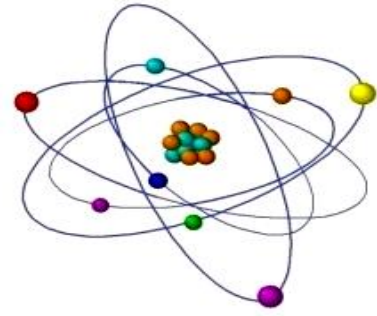


# 3D VISUALIZATION OF NUCLEAR DAMAGES IN HISTONE H2B-GFP TAGGED HE-LA CELLS: POST-IRRADIATION IMAGING



<sup>1,2</sup>Lili Nadaraia\*, <sup>1</sup>Veriko Okuneva,  
<sup>1,3,4</sup>Mikheil Nanikashvili, <sup>1</sup>Pavel Tchelidze

<sup>1</sup> Scientific and Education Center by Carl Zeiss, New Vision University, Georgia

<sup>2</sup> Republic Center of Structure Research, Georgian Technical University, Georgia

<sup>3</sup> Georgian Scientific Industries LLC, <sup>4</sup> Georgian Science Innovation Organization, Georgia

<https://doi.org/10.63465/rrs520258981>

\*Corresponding author: Email: nadaraia@gtu.ge

**ABSTRACT:** *Here we suggest visualization of the spatial nuclear changes using unique He-La cell line stably expressing histone H2B-GFP fused protein as a chromatin signature. To do this we offered Carl Zeiss LSM900 confocal microscope-based acquisition of Z-stacks, coupled with the 3D image reconstruction and rendering using ZEN and UCSF Chimera. Our recently displayed 2D images, showed that  $\gamma$ -irradiation leads to spatially very complex nuclear changes, so that one can easily defined that 2D approach is largely unable to yield precisely analyzed results. Meaning that in our experiments  $\gamma$ -irradiation in dose of 30 Gy led to the drastic nuclear deformations, followed by fragmentation and massive emergence of multi-nucleated cells, we resorted to only reliable analytical way, namely to 3D visualization and modeling approach. Our interest was spotlighted on the  $\gamma$ -irradiation induced nuclear and nucleolar changes due to: (i) the cell nucleus is the largest, highly ordered but dynamic cellular compartment, housing around 1.5 m DNA strand in common genome length. Although giant sizes complete genome is spatially precisely arranged being compacted inside confine of average 15-20  $\mu\text{m}$  in diameter. Such a big sizes expose nuclear chromatin to natural but potentially damaging factors, particularly to  $\gamma$ -irradiation. Therefore, it is crucial to follow dynamics and degree of morphological damages, under permanent monitoring of nuclear viability; (ii) the common length of rDNA chromatin clustered as tandems of r-genes is also large enough to represent easily accessible target after being exposed to  $\gamma$ -irradiation. Because, the key function of the nucleolus, as a ribosome factory, plays central role in whole cellular metabolism, monitoring of related structural damages are particularly challenging.*

*Using 3D imaging/modeling hardware combined with UCSF Chimera we managed to describe in details specific nuclear/nucleolar damages aroused as a consequence of  $\gamma$ -irradiation with dose of 30 Gy. In fact, present work represented first attempt to show modern digital 3D visualization facilities in order to motivate young Georgian bio-medical scientist to use available software and other microscopy-based digital techniques for the living and fixed cell/tissue 3D/4D imaging. Importantly, all these facilities are locally available at "Open Platform for Advanced Microscopy" established in New Vision University "Scientific and Education Center by Carl Zeiss".*

**Key word:** He-La Cells, 3D-visualization, irradiation, nuclear damages, imaging

## INTRODUCTION

Why Nucleolus? The nucleolus, a vital nuclear compartment, orchestrates ribosome biogenesis by producing polycistronic transcripts. It integrates gene-rich chromosomal domains, forming nucleolus-

associated DNA (naDNA). The common length of rDNA chromatin clustered as tandems of ribosomal genes (rRNA genes, rDNA chromatin, r-genes) is also large enough to represent prime target after being exposed to UV and  $\gamma$ -irradiation [15-27]. The nucleolus hosts molecular machinery that guides the transcription of ribosomal genes, pre-rRNA processing, and ribosome assembly. It is generally accepted that organized as nucleolus, sites of localization and transcription of r-genes, together with products of their activity, represent highly sensitive sensors of cellular stress. Therefore, various chemical stress factors (including anticancer drugs) that inhibit different steps of ribosome biogenesis have been used as the most suitable tools to study structure-functional aspects of the nucleolus in compliance with entire cell metabolism [28-38]. Thus, previous studies using the rRNA synthesis chemical inhibitor Actinomycin D (AMD) showcased drastic reorganization caused by intra-nucleolar movement of nucleolar constituents, namely fibrillary centers (FCs) and dense fibrillary component (DFC) due to concerted contraction of nucleolus-associated DNA chromatin (NAC) [14].

Because, the key function of the nucleolus, as a ribosome factory, plays central role in whole cellular metabolism, monitoring of related structural damages are particularly challenging. While chemical inhibition has been extensively investigated [28-38] the impact of physical DNA damage on nucleolar organization remains less understood.  $\gamma$ -Irradiation, a powerful inducer of DNA single- and double-strand breaks in plant and animal cells, causes large-scale nuclear deformation, chromatin condensation, and apoptosis [13, 27, 39-42]. However, its specific effects on nucleolar structure, particularly on NAC dynamics and FC and DFC complex (hereafter FC/DFC assembly), are poorly characterized. Given nucleolar high rDNA content and its involvement in metabolic stability, rDNA clusters are prime targets for  $\gamma$ -irradiation-induced damage. It is therefore critical to determine whether such physical damage induces nucleolar segregation pattern similar to those observed during chemical inhibition [14, 28-30, 34, 35] or if alternative structural adaptations occur. Furthermore, the role of nucleolar proteins in mediating these responses remains an open question, with particular interest in the behavior of Pol I associated architectural transcription factor UBTF and pre-rRNA early processing factor fibrillarin. It is well documented that UBTF has long been acknowledged as the most specific marker of FC, while fibrillarin became recognized as widely used marker of DFC [14, 50].

Why  $\gamma$ -Irradiation? Having broadly explored inactivation dynamics through chemical r-genes transcription inhibition, here we planned to delve into the nuclear and nucleolar molecule-structural reorganization under severe DNA damage by physical factor  $\gamma$ -irradiation that induces single- and/or double-strand breakages. Our idea posits on presumption that  $\gamma$ -irradiation-induced nucleolar inactivation dynamics can mirror changes observed with AMD induced rRNA synthesis inhibition. For example, focusing on nucleolar changes, we can investigate if physically damaged naDNA exhibits similar movement as those after induced chemically. Correspondingly, this report deals with the nuclear/nucleolar 3D reorganizations under severe DNA damage induced by  $\gamma$ -irradiation using 30 Gy dose. As the most reliable model justifying nuclear/chromatin damages as well as aiming to future radiobiological/bio-medical application we employed a cancer cell line, namely He-La cells stably expressing histone H2B-GFP fusion proteins [14]. Based on data obtained in previous study [51] we applied experimental model that involves 3D imaging of possible post- $\gamma$ -irradiation nucleolar inactivation monitoring intra-nuclear/intra-nucleolar changes developed within 0 - 72 hours' period of post-irradiation imaging.

In summary, our study investigates the three-dimensional structure and dynamics of nuclear and nucleolar reorganization following DNA damage induced by  $\gamma$ -irradiation. Using post-radiation time-lapse imaging over 72 hours, we analyzed nuclear deformation, chromatin remodeling, and apoptotic events in He-La cells stably expressing histone H2B-GFP. Volume light microscopy in living and fixed cells revealed key changes, including chromatin clumping, nuclear cleavage, and multi-nuclear cell formation. To assess nucleolar reorganization, we visualized FCs, that represents transcriptionally active rDNA sites, through anti-UBTF immunolabeling in fixed H2B-GFP HeLa cells. For immunolabeling of pre-rRNA early processing nucleolar sites, structured as DFC we applied anti-fibrillarin immunostaining.

Undeniably, the most informative digitalized 3D/4D approaches are highly important for science and education as all they are properly aligned with modern bio-medical tasks [14, 36]. Notable, that currently, baccalaurean, postgraduates and PhD students in the majority of Georgian Universities are

unable to use corresponding computed 3D/4D microscopy analysis in any kind of scientific work. Obviously, that the major obstacle that conditioned extremely limited scientific application of 3D/4D microscopy in Georgia is very high price of corresponding hard and soft ware. Therefore, another important goal of presented study is to show the simple way how to overcome mentioned obstacles and to demonstrate where and how young scientists can learn and use our modern instrumentals for 3D/4D digital microscopy imaging. Here we demonstrated effectiveness of widely spread GFP-based in situ labeling method as well as modern imaging techniques including optical tomography approach. All these techniques gained high priority being combined with related free software like “ImageJ” and UCSF Chimera. Most importantly, guided by modern microscopy strategies, “Scientific and Education Center by Carl Zeiss” (SECCZ) at New Vision University (NVU) can play a teaching/developmental role for early career investigators looking for a home for their progressive ideas. So, we seek to create a mentoring and cutting-edge scientific environment, encompassing young specialists and helping elevate the impact of their research through now available modern digital 3D/4D light and electron microscopy approaches.

## MATERIAL AND METHODS

We utilized histone H2B-GFP transfected He-La cells obtained from Prof. O. Piot (University of Reims Champagne-Ardenne, France). Importantly, that now this unique cell line is in open access at NVU SECCZ. As our main goal was study of changes in nuclear and nucleolar morphology the choice of this cell line was based on their distinct features. Among most important features were: (i) the nuclear fluorescence of these cells demonstrated high stability, crucial for obtaining brightly fluorescent, of post-irradiated cells; (ii) these cells exhibited prominent intra-nucleolar fluorescence, identified as nucleosomal domains with the ultrastructural appearance of intra-nucleolar condensed chromatin (ICC). This characteristic was vital for our study; (iii) He-La cells are known for their large FCs associated with prominent DFC zones, aiding in the immunocytochemical discrimination of nucleolar sub-territories involved in r-gene transcription and pre-rRNA processing.

All basic experimental conditions, such as cell culture maintenance, growing and seeding quantitative parameters of cells submitted for working culture irradiation, irradiation machinery and regime, as well as digital microscope 3D image acquisition and 3D reconstruction/ visualization parameters were performed in full accordance with early reported data [51]. Additionally, in order to record specific 3D nucleolar changes in two nucleolar components (NCs) i.e. FC and DFC we employed anti-UBTF and anti-Fibrillarin immunocytochemical staining according presented below protocols (see section 2.2.)

### Short Description of Irradiation procedure and Post-Irradiation Imaging.

Before being submitted to  $\gamma$ -irradiation, cells were briefly rinsed with PBS (3 times during 5 min), immersed in fresh medium, and the dishes were delivered to “GUPOS”  $\gamma$ -installation. Irradiation of cells was conducted directly in Petri dishes at a temperature of 35 $\pm$  20C. As a source of  $\gamma$ -irradiation, the Cs137 isotope with a dose of 1.1 Gy/min has been utilized. After irradiation, cells were washed in PBS (3x5 min), returned to the cultivation media, and then s  $\gamma$ -installation subjected to time-lapse imaging during 0-72 h using Carl Zeiss (Germany) LSM 900 microscopes equipped with Axio Observer Z1/7 inverted microscope and AiryScan 2 augmented resolution device as it was recently described [51].

### Post-Fixation 2D/3D Visualization of UBTF and Fibrillarin

Imaging of UBTF labeled cells is widely used to identify under-condensed active, potentially active and inactive rDNA genes folded into the structure of interphase FC and metaphase NORs [14, 36]. Meanwhile, imaging of anti-Fibrillarin labeled cells was performed because it is present at high concentration within the DFC where its rRNA methyl transferase activity is required for rRNA processing [14, 50]. These characteristics allowed to follow FCs and DFC as well as to study of their 3D modifications induced by  $\gamma$ -irradiation. For post-fixation imaging of anti-UBTF and anti-fibrillarin

mono- and double-immunolabeled cells we used primary monoclonal antibody conjugated with AlexaFluor488 and AlexaFluor594, both purchased from Santa Cruz Biotechnology (USA). This type of antibodies allows by mono-immunolabeling to use only one block for nonspecific binding in normal goat serum (NGS, Novex, USA) as well as avoid incubation with biotinylated secondary antibody by mono- and double-immunolabeling, thus making duration of immunostaining procedure notably shorter. Testing primary monoclonal antibodies conjugated with AlexaFluor594 (anti-UBF/F9 fragment and anti-fibrillarin) and AlexaFluor488 (anti-fibrillarin), we elaborated two protocols that sufficiently differ from early used schemes [14, 34].

By mono-labeling both, anti-UBTF as well as anti-fibrillarin procedures included four similar steps, namely: (i) after brief rinsing in PBS  $\gamma$ -irradiated samples were fixed at room temperature (RT) during 10 min in 4% PAF diluted in PBS and adjusted to pH 7.2-7.4 by 0.1N NaOH and rinsed repeatedly in PBS (3x5 min); (ii) cells were permeabilized by incubation in 1% TritonX-100 diluted in PBS during 5 min, and extensively washed in PBS; (iii) to block nonspecific binding, cells were incubated in 10% NGS in PBS during 60 min at RT; (iv) after removing NGS the cells were covered either by mouse anti-UBF/F-9 fragment or by mouse anti-fibrillarin AlexaFluor594 conjugated primary antibodies diluted (1:20) in PBS containing 1% NGS overnight at 4oC. After cells were washed with PBS (3x5 min), selected samples were submitted to LCM imaging according procedure described in 2.4.

For simultaneous visualization of UBTF (in red) and fibrillarin (in green) we utilized double labelling according protocol that includes following 6 steps: (i) as it was described above, briefly rinsed  $\gamma$ -irradiated cells were fixed in 4% PAF and rinsed again (ii) cells were permeabilized in 1% TritonX-100 prepared in PBS during 5 min, and extensively washed in PBS; (iii) to block nonspecific binding, cells were incubated in 10% NGS in PBS during 60 min at RT; (iv) after removing NGS the cells were covered with anti-UBF AlexaFluor594 conjugated primary antibodies diluted (1:20) in PBS containing 1% NGS overnight at 4oC; (v) after rinsing in PBS (3x5 min) cells were secondly incubated in 10% NGS during 60 min at RT; (vi) NGS was removed and cells were covered with anti-fibrillarin AlexaFluor488 (1:20) dissolved in PBS containing 1% NGS over night at 4oC. Being washed in PBS cells were submitted to LCM imaging directly in culture boxes.

### 3D Reconstruction and Visualization

As we reported recently for preliminary time-lapse analysis and visualization behavior of living cells damaged by  $\gamma$ -irradiation, obtained time series were transformed into 2D movies using ZEN 3.0 software [51]. For control, we used high-magnification LSM imaging conducted before  $\gamma$ -irradiation treatment. Importantly, living cell imaging allowed us to identify significant for 3D imaging points so that worth for visualization, drastic changes were detected during 48 – 72 hours of post-irradiation image acquisition period. Next, points of interest were extracted from whole dataset in order to visualize the changes in nuclear/nucleolar structural parameters, as well as coalescence of ICC clumps during  $\gamma$ -irradiation in 3D. The Z-stacks have been collected using up to 70 virtual sections taken with 0.3  $\mu$ m step between individual section. Cells were examined and imaged in 512x512 pxl format. 3D models were generated using ZEN 3.0, “ImageJ” and UCSF Chimera. For this, obtained LSM volumes were exported to mentioned software for 3D reconstruction, rendering, visualization and modelling. At the final stage rendered 3D models were analyzed using rotation/tilting options in order to select most appropriate foreshortenings of resulted models.

## RESULTS

The 2D images and 3D model of the nuclear exterior in control cells, that includes global shape and outline are presented on Fig. 1, a-k. Cells are exclusively mononuclear, while nearly all nuclei revealed roundish or elongated shape, mostly with slightly wave-like contours (Fig. 1, a-c). Nuclei revealing more or less profound invagination were observed just occasionally. Notably, cultures examined entirely showed absence of multi-nuclear cells. Another credible criterion indicating the good “health” of cells in cultures was abundancy of dividing cells which were at different stages of mitosis (Fig. 1, a, c). Meanwhile, in control samples apoptotic cells were rarely seen (Fig 1, b).

Nucleoli were appeared against the brightly fluorescent chromatin as large dark, roundish or elongated territories (Fig. 1, a-c). The nucleoli were well detectable due to presence of prominently

fluorescent ring of peri-nucleolar condensed chromatin (PCC) delineating boundary of nucleolar territory. Nucleolar contours were predominantly roundish, while nucleoli with elongated or irregular outlines also could be registered. Nucleolar perimeter and interior regularly showed fluorescence of the NAC, presented in the form of intra-nucleolar inclusions i.e. condensed/nucleosomal chromatin cords (ICC cords) extending from PCC shell deep inside the nucleolar territory. PCC consistently exhibits higher fluorescence than ICC. Even at low magnification, it became obvious that nucleoli contain histone H2B-GFP positive structures of different sizes and appearances attributed to ICC. ICC inclusions have slightly less intense labeling than chromatin fluorescence (Fig. 1, a, c).

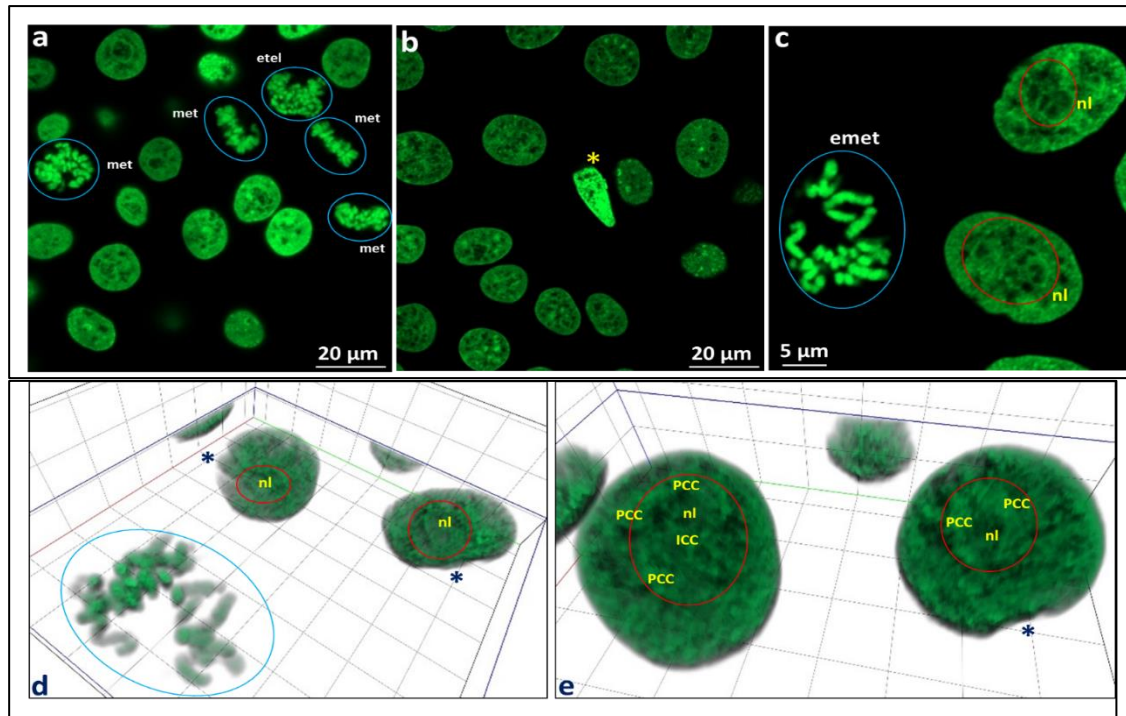


**Fig.1 Structural features of nuclei in control He-La cells stably expressing histone H2B-GFP fusion protein**

Fig. 1, a – c – note abundance of mitotic cells (taken in blue circles on Fig. 1, a, c). Occasional apoptotic cells are also seen (marked by yellow star on Fig. 1, b). At low magnification nuclei mostly have roundish or elongated appearance and smooth contours (Fig. 1, a, b), while at higher magnification nuclei can reveal wave-like outlines due to small indentations (Fig. 1, c). Signs of more or less deep invagination or cleaved nuclei absent. Even at low magnification nucleolar territory is well recognizable by presence of profound ring of PCC that delineates nucleolar perimeter (see upper left nucleus on Fig. 1, a). At higher magnification intensively branched ICC network (outlined by red circles) became especially obvious (Fig. 1, c). Fig. 1, d, e - 3D models of nuclei generated by ZEN software, using aligned: (i) volume rendering; (ii) transparency mode by (iii) variable thresholds correspond to mitotic cell and nuclei depicted. Nucleolar territories (nl) on both images are outlined by red circles. Nuclear periphery that shows small indentations are marked by stars on Fig. 1, d, e. Meanwhile, on Fig. 1, e PCC and ICC components of NAC are well recognizable. In spatial view 3D network formed by ICC is undeniable see left nucleus showed on Fig. 1, e). Note also thick PCC shell around nucleolus in right nucleus. Abbreviations: emet – early metaphase; etel – early telophase; met – metaphase; nl – nucleolus.

In 3D it became especially well recognizable that PCC forms around confines of the nucleolar territory prominent, solid, or locally disrupted shell (Fig. 1, d, e). Meanwhile, ICC forms intensively branching network connecting with PCC shell via many sites, both being integrated into unit NAC system. Indeed, 3D visualization and rotation of models reveal multiple cord-like structures emanating from the PCC shell. These "off springs" protrude inside the nucleolar territory, creating the impression of discrete ICC clumps on individual sections. Thus, after 3D modeling the existence of a unit ICC network that structurally communicates with the PCC shell became undoubted (1, d, e).

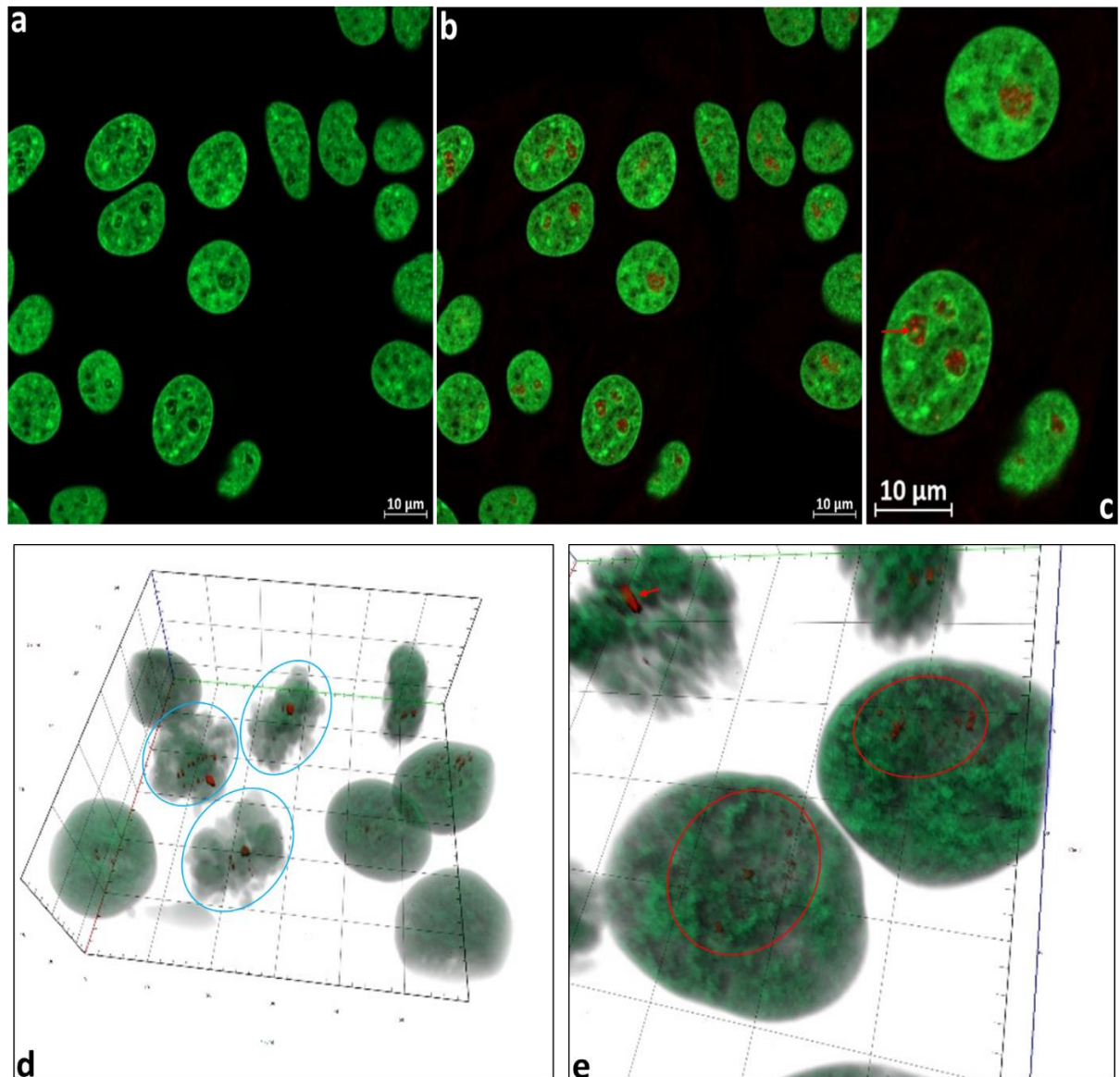
Regarding to 2D distribution and 3D organization of UBTF and fibrillarin positive NCs in fixed control cells we clearly visualized the relationships between the NAC and anti-UBTF immunolabeling. First of all, we detected UBTF fluorescence inside H2B-GFP positive intra-nucleolar network of NAC (Fig. 2, a-c). As a consequence, in 3D views the spatial interplay between GFP positive NAC and UBTF positive fluorescence became especially obvious, so that intensively branched ICC network appeared always intermingled with FCs (Fig. 2, d, e). Such a proximity of ICC and anti-UBTF tags shows the intimate link between nucleosomal, most probably non-ribosomal chromatin and relaxed r-chromatin folded into structure of FCs, i.e. interphase counterpart of mitotic NORs [14]. Moreover, we observed that ICC clumps, which were linked to UBTF positive FCs, were also attached to a PCC shell and created a bridge between these chromatin components. Hence, observing spatial integration of FCs into the whole network of NAC confirms early described tight link between nucleosomal and non-nucleosomal fractions of naDNA [14].

Secondly, histone H2B-GFP He-La culture allowed us to address also to 2D imaging of fibrillarin distribution and aligned imaging of 3D relationship of fibrillarin and UBTF complex with NAC (Fig. 3, a-g). In 2D fibrillarin positive labeling was always concentrated in cord-like structures that seemed were in tight association with NAC (Fig. 3, a-c). Corresponding 3D models are displayed on Fig. 3, d, e. Concomitant 3D visualization of the UBTF and fibrillarin couple as well as their relationship in control cells, produces clear evidence that these nucleolar proteins are closed together (Fig. 3, f, g). The close structural link between these nucleolar subdomains suggest the putative position of FC/DFC assembly inside ICC network. By this, fibrillarin positive DFC “covers” the chain-/necklace-like organized groups of FCs. Therefore, inside these units, discrete FCs (or their groups) are looking like embedded into a cord-like mass of DFC (Fig. 3, f, g).

As we described earlier, the post-irradiation time-lapse imaging showed that most profound nuclear/nucleolar alterations were detected within 48 – 72 hours’ period of post-irradiation image acquisition [51]. Correspondingly, here we exclusively focused on 2D images and 3D models of  $\gamma$ -irradiation-induced nuclear and nucleolar changes that develop during above mentioned post-irradiation time (Fig. 4, a-c and 5, a-f). It became clear that at this experimental point  $\gamma$ -irradiation in dose 30 Gy inflicts severe damage to nuclear chromatin structure displayed on Fig 4, a-c. Collected Z-stacks involving changes developed to the 72 hours revealed a three-stage process of nuclear evolution: (i) progressive nuclear invagination leading to a lobulated shape (Fig. 5, a, b); (ii) asymmetric nuclear fragmentation into unequal-sized micronucleoli (Fig. 4, a-c; 5, c-f); (iii) following asynchronous apoptotic nuclear degradation (Fig 4, a-c). Interestingly, that even after 72 post-irradiation hours a significant part of survived cells are mononuclear, while resting part can abundantly reveal deep invaginations and/or lobed nuclei. Nuclei slightly resembling control ones i.e. roundish with more or less smooth outlines, also existed, however we observed them just occasionally (Fig. 4, a, b).

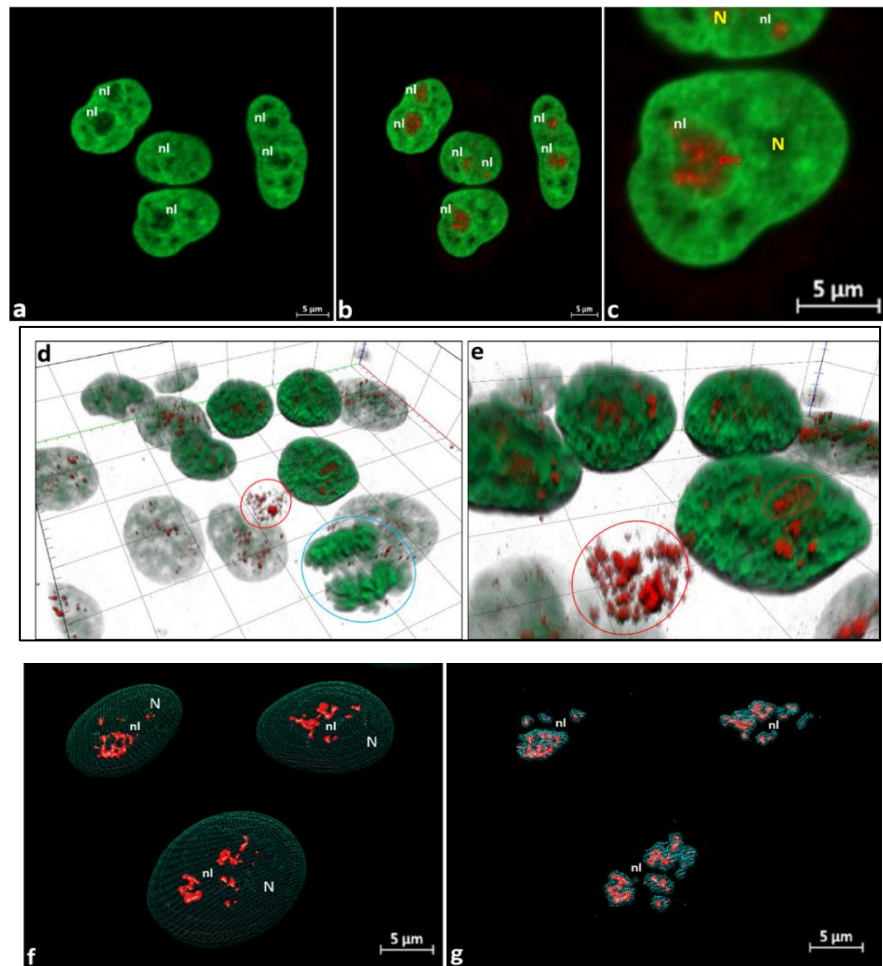
Additionally, we interested whether  $\gamma$ -irradiation induced nucleolar inactivation pattern resembling NAC and FC/DFC assembly rearrangements observed with chemical inhibitors and called nucleolar segregation and capping [28-30, 34, 35]. As a rule, applied in our study dose of  $\gamma$ -irradiation led to the specific transformation of FCs and FC/DFC assembly. Unlike classical pattern of rRNA synthesis inhibition by chemical agent AMD, nucleolar segregation or capping was not observed. However, we registered asymmetric enlargement of one to three (rarely even more) FCs, acquiring giant but spherical form, which never been reshaped into crescent-like caps.

These peculiar entities always stud inside nucleolar territory, remaining spherical and being shifted to the interface between PCC shell and nucleolus [Fig. 4, b; 5, c-f). Interestingly, groups comprised several UBTF positive FCs which were of sharply smaller sizes could always be detected. Likewise, DFC never acquired cap-like structure always retaining its cord-like spatial arrangement (Fig. 5, b). Remarkably, that even after 72 hours, nucleoli remained large, irregularly shaped, and retained multiple FCs, suggesting a pre-segregated state rather than complete nucleolar segregation [14]. By this we conclude that even after 72 hours of post- $\gamma$ -irradiation imaging period 30 Gy dose is unable to disassemble FC/DFC unity.



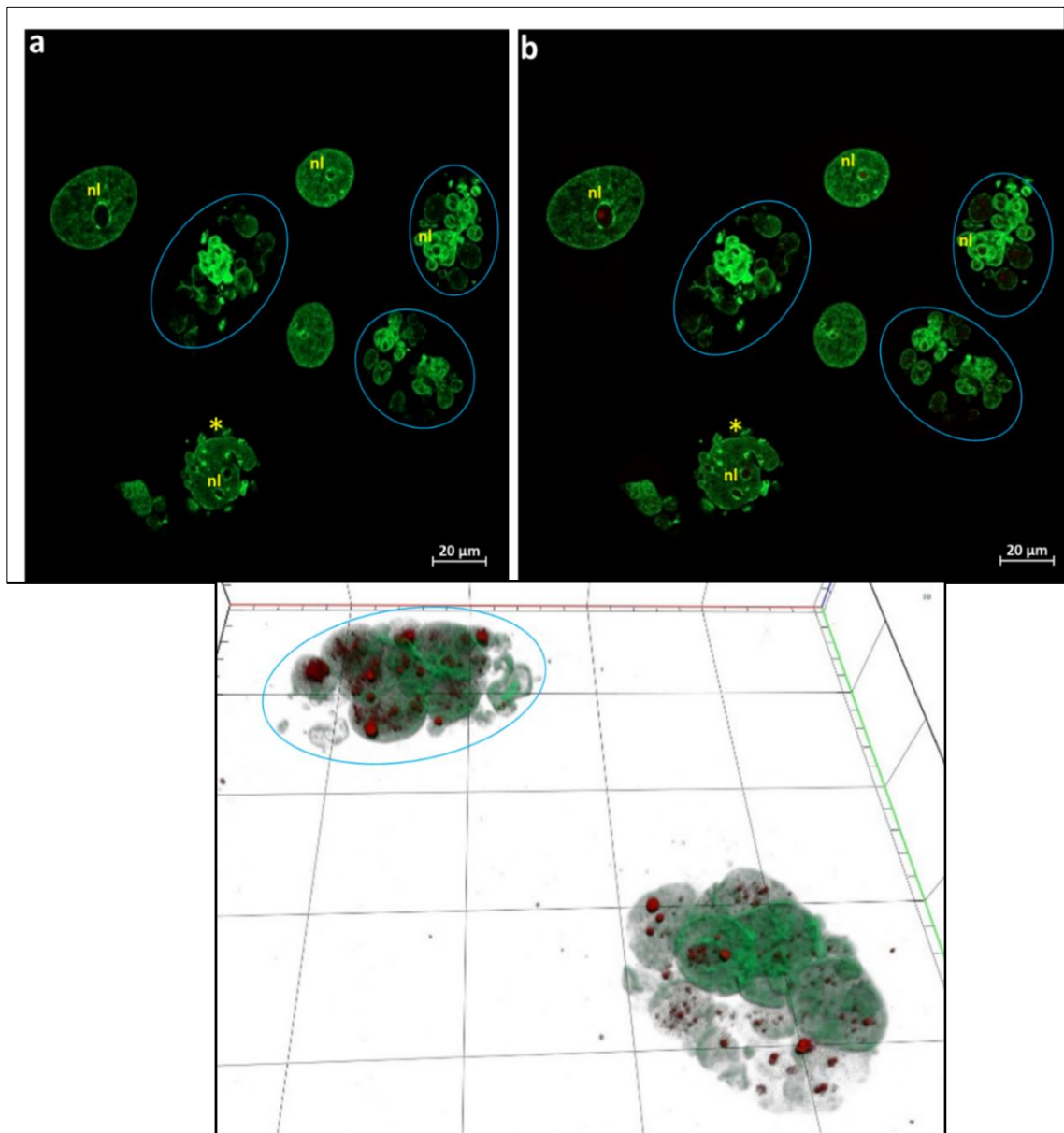
**Figure 2. Nuclear morphology in control histone H2B-GFP permanently transfected He-La cells submitted to anti-UBTF immunostaining**

Fig. 2, a – c - note prominent nuclear polymorphism, showing that beside roundish nuclei the elongated ones as well as nuclei with slightly curved contours were detected. Fig. 2, a – low magnification; histone H2B-GFP transfected He-La culture before immunolabeling. Even at low magnification nucleolar inclusions of ICC were regularly seen. Fig. 2, b – overlay of GFP and anti-UBTF labels; after immunostaining anti-UBTF label was exclusively concentrated inside nucleolar territory. Fig. 2, c – overlay of GFP and UBTF positive structures at higher magnification; integration of UBTF positive entities into unit NAC network became clear; note that red arrow indicates site of co-localization of green and red fluorescence, i.e. ICC and UBTF containing structures. Note also that PCC fluorescence was brighter than those of ICC. Fig. 2, d, e - ZEN generated 3D models reconstructed and rendered using same options as it was described on Fig. 1, d, e. 3D images clearly show integration of UBTF positive FCs into NAC network. Fig. 2, d – low magnification; UBTF positive signal was exclusively restricted by FC and NORs (mitotic cells were taken in blue circles). Fig. 2, e – high magnification; spatial visualization of link between FCs and NAC became better visible; red circles delineate nucleolar territory. Red star indicates large NOR.



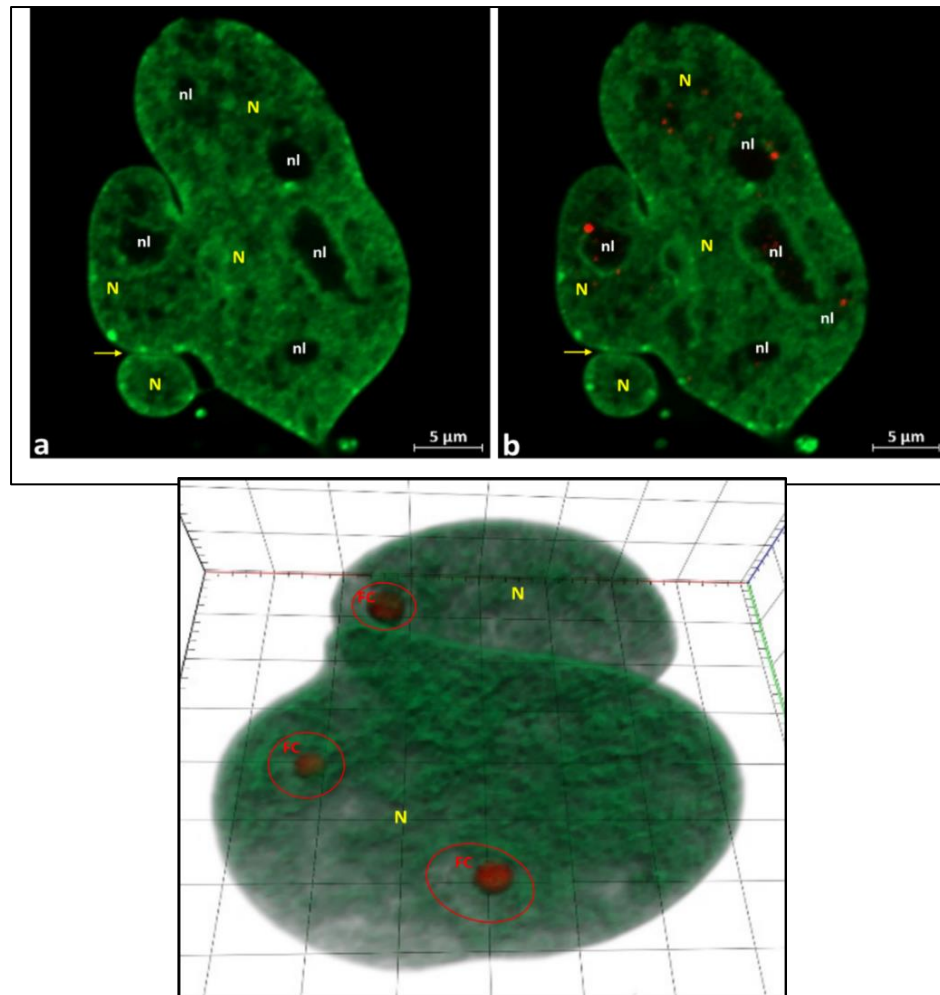
**Figure 3. Nuclear morphology in non-irradiated (control) histone H2B-GFP permanently transfected He-La cells submitted to anti-fibrillarin immunostaining. Note profound nuclear polymorphism, witnessing presence of cells with elongated/curved nucleolar outlines**

Fig. 3, a – low magnification; histone H2B-GFP transfected He-La culture before immunostaining. Both, nucleolar inclusions of ICC as well as well pronounced PCC ring were presented. 3, b – overlay of GFP and anti-fibrillarin positive structures; after immunostaining anti-fibrillarin label was concentrated within nucleolar territory. Fig. 3, c – overlay of GFP and fibrillarin positive structures at higher magnification, confirming integration of cord-like fibrillarin containing structure (DFC) into NAC network. Fig. 3, d, e - 3D models reconstructed and rendered using same options as it was described on Fig. 1, d, e. 3D models showing integration of fibrillarin positive DFC into NAC network. Fig. 3, d – low magnification; fibrillarin positive signal was gathered only inside DFC. Mitotic cells were taken in blue circle, while red circle outlines the region of anti-fibrillarin signal localization inside the nucleus that was not transfected, i.e. nucleus that don't emit green fluorescence of chromatin. Mitotic chromosomes were free from anti-fibrillarin label. Fig. 2, e – high magnification; left, large red circle delineates the anti-fibrillarin signal inside not transfected nucleus, while left, small red circle demonstrates cord-like organization of DFC. Fig. 3, f, g - 3D models, generated by “Chimera” software. Fig. 3, f - demonstrates spatial distribution of UBTF positive signal (red), showing necklace-lake organization of FCs inside nucleus (green) Fig. 3, g - 3D model, confirming intimate association of UBTF positive FCs and fibrillarin positive DFC (blue) in form of FC/DFC assembly. This figure shows only FC/DFC assembly which was extracted from nuclear interior. N – nucleus; DFC – dense fibrillar component; other abbreviations are same as on previous images.



**Figure 4. Effect of 30 Gy  $\gamma$ -irradiation upon nuclear structure of histone H2B-GFP transfected He-La culture**

Images correspond to 72 hours of post-irradiation imaging period. Fig. 1, a – this image was taken before anti-UBTF immunostaining; 1, b – same nuclei after anti-UBTF immunostaining. Note, that beside severely damaged cells with cleaved nucleus (marked by yellow star) and multi-nuclear cells (taken in blue circles) we registered “survived” mononuclear cells which nuclei had close to control appearance. In all cases (including nucleolated fragments in multi-nuclear cells) nucleolar territory can be easily identified. Note also UBTF positive structure (FC) inside nucleolus of upper left cell. Fig. 4, c – ZEN generated 3D models reconstructed and rendered using same options as for cells showed on Fig. 1, d, e. These 3D models display severely damaged multi-nuclear cells (taken in blue circles) after anti-UBTF immunolabeling. Note spatial rearrangement of UBTF positive structures into nuclear fragments appeared at 72 hour of post- $\gamma$ -irradiation image acquisition. Signs of disruption and chaotic redistribution of FCs inside nucleolated fragments were obvious.



**Figure 5. Severely damaged mononuclear histone H2B-GFP expressing He-La cell with lobbed/cleaved nucleus before (Fig. 5, a) and after (Fig. 5, b) anti-UBTF immunostaining.**

Early stage of nuclear fragmentation (yellow arrows). Fig. 5, b – after anti-UBTF immunostaining picture of disruption/dispersion of FCs became undisputable. Fig. 5, c- e. Early step of nuclear fragmentation: formation of two closely located nuclear fragments appeared at 72 hours of post-irradiation imaging period. Images were taken before (Fig. 5, a) and after (Fig. 5, b, c) anti-UBTF immunostaining. Fig. 5, a – nucleolar territories surrounded by prominent PCC ring are well recognizable. Fig. 5, b, c - two not successive section planes extracted from Z-stack in order to demonstrate giant UBTF positive FCs in all nucleoli. Note exclusive intranucleolar localization of FCs that link to PCC. Note also direct structural contact between FC and protrusion of PCC into nucleolar territory. Importantly, we never observed classical picture of nucleolar segregation and capping. Fig. 5, f - the same nuclei as on Fig. 5, c – e, demonstrating early stage of nuclear fragmentation. This ZEN generated 3D model was reconstructed after anti-UBTF immunolabeling. Obviously, UBTF positive FCs increased to giant sizes, however still stud spherical and located inside nuclear territory (outlined by red circles). We never observed reshaping of spherical FC into crescent-like caps. All abbreviations are same as on previous images.

## DISCUSSION

Our major goal was to demonstrate the structural and functional interplay between  $\gamma$ -irradiation induced r-gene inactivation and large-scale modifications of intra-nucleolar structure with particular regard to possible territorial reorganization of NAC and related structures. Correspondingly, the present study focuses not only on profound nuclear and chromatin destruction but also on the reorganization of NAC, particularly ICC and PCC, in compliance with behavior of FC/DFC assembly, under severe DNA damage induced by  $\gamma$ -irradiation. Regarding nucleolar analysis, the key aspect to consider in this study was the impact of the less studied physical factor, particularly  $\gamma$ -irradiation upon nuclear/nucleolar chromatin structure and behavior of FC/DFC assembly.

As UBTF is specifically associated with active under-condensed rDNA genes it was extensively used as reliable marker of FCs in experiments applying either GFP tagging or immunostaining [14, 52, 53]. Meanwhile, fluorescent detection of fibrillarin, based on both GFP and immunolabeling approaches has widely been adopted by addressing to early pre-rRNA early processing nucleolar sites [14, 50]. Specifying the  $\gamma$ -irradiation induced UBTF and fibrillarin redistribution pattern resulting in particular behavior of FC/DFC assembly we concluded that the most peculiar changes we registered are: (i) never observed the picture when irregularly shaped nucleoli transform into small, sharply outlined and dense entities as it usual by nucleolar segregation. On the contrary, even passing through 72-hour post-irradiation image acquisition period in all survived cells nucleoli stud large enough and irregularly shaped; (ii) absence of typical segregation, expressed in transformation of FC/DFC assembly into crescent-like nucleolar caps, although  $\gamma$ -irradiation can induce transcription inhibition [46]. FCs along with tightly associated DFC “cover” stud always inside nucleolar territory; (iii) distinct demonstration using 3D models that despite asymmetrically enlarged one or two clearly spherical FCs, spatial organization of these r-chromatin containing NCs looked like drastically different as few extremely small UBTF positive entities stud permanently beside giant FCs; (iv) fibrillarin positive DFC undergoes minor changes still exhibiting cord-like fluorescence, even being collected through 72 hours acquisition period; (v)  $\gamma$ -irradiation unable to disassemble FC/DFC complex, so that giant as well as small FCs were always either fully or in part “wrapped up” by fibrillarin containing DFC.

While following the post-irradiation interplay of the NAC system with the FC/DFC assembly we emphasized that posing as an integral part of the nucleolus, the functional role of NAC still needs to be investigated. This largely increased the credibility of our data, indicating their particular significance as a novel insight in the intra-nucleolar dynamics of NCs. It is well established that, once formed, the nucleolus remains intimately associated with the physiological state of NAC. The structural remodeling of NAC can affect the spatial arrangement of active r-genes and the global organization of the nucleolar factories. As it was suggested, most likely, NAC constituents do not contain r-genes due to the absence of specific accessory factors necessary for the maintenance of the template in an under-condensed/open state [14, 34, 53]. Hence, the absence of UBTF facilitate the keeping of the nucleosomal structure of ICC and PCC. How NAC responds to the action of DNA-damaging factors, particularly radioactive exposure, remains largely unknown. It seems much more problematic to understand whether NAC still retains the ability to condense and drive the movement of NCs while naDNA undergoes  $\gamma$ -irradiation breakage and degradation.

Although the dynamics of  $\gamma$ -irradiation-induced NAC changes largely mirror inactivation pattern observed in AMD-induced rRNA synthesis inhibition, behavior of FC/DFC assembly completely differs from reorganization pattern observed by chemical inhibition of the nucleolus. In

cells exposed to  $\gamma$ -irradiation of 30 Gy dose, ICC structures gradually coalesce, being stepwise shifted towards PCC and forming coarser but increasingly fluorescent clumps. Most probably, despite severe naDNA damage ICC retains mobility and contraction, presumably driving tightly linked FCs to delocalize, as it was registered in AMD treated Histone H2B-GFP He-La cells [14].

Undoubtedly, massive and striking nuclear changes delay until 48 – 72 hours. Accordingly, we expected remarkable changes in NAC and FC/DFC assembly to these experimental points. Indeed, after treatment by 30 Gy dose drastic changes increasingly appear during 24-48 hours of post-irradiation image acquisition period. Here we revealed the bulk of highly deformed nuclei in both mononuclear and multi-nucleated cells, including apoptotic ones. In all survived mononuclear cells that reveal comparative resemblance with control morphology the integration of FC/DFC into NAC unit remains unchanged. Interestingly, that even highly damaged, multi-nucleated cells we could see nucleoli, but not in all nuclear fragments. Such nucleoli could exhibit deformed shape while UBTF and fibrillarin fluorescence remains quite bright.

Meanwhile, post-irradiation changes over 48 - 72 hours enabled the revealing of the nuclear/nucleolar evolution stages. For this, we resorted to key experimental points that were identified for detailed analysis. As a consequence, we convinced that 30 Gy dose of  $\gamma$ -radiation is unable to disassemble the FC/DFC and NAC unity despite deep and invertible destruction of the nucleus and nucleolus, that leads to nuclear fragmentation, cellular multi-nucleation with following apoptotic degeneration, nucleolar disruption and finally to cellular death. Importantly that NAC and FC/DFC unity is conditioned through nucleolar condensed chromatin, particularly ICC. Undoubtedly, one more intriguing issue worth further engagement is that even severe DNA damaging by 30 Gy regime indicated the maintenance of naDNA to contract thus drive nuclear and nucleolar dynamics. Therefore, trying to explain delayed nucleolar changes and relative stability of NAC and FC/DFC system during longer time, we could hypothesize that densest nucleolar composition can serve somehow as kind of “shield”. In turn, due to intra-nucleolar localization, hence being possibly better protected, r-chromatin can remain viable longer than some, “less protected” nuclear functional compartments as well as cytoplasmic organelles. At least this suggestion is worth to be included in our planned next experiments aiming detection of single and double DNA strand breakages.

Moreover, our study specifically focuses on the mechanisms of multi-nuclear cell formation and nucleolar changes accompanying asynchronous apoptotic destruction. Although emergence of the multi-nuclear cell and asynchronous apoptosis in nuclear cells was frequently registered after UV and  $\gamma$ -irradiation [6, 8, 54], up to date, there is no comprehensive explanation of underlying sub-cellular and molecular mechanisms. Importantly, our results enabled to hypothesize at least one of the possible sub-cellular mechanisms of multi-nuclear cell emergence. We think that described processes unfold in distinct stages, hence presenting possible underlying cellular mechanisms. The consequential steps of post-irradiation dynamics of this process may develop in two steps. Initially, the formation of deep invaginations of the nucleus takes place that imparts a cleaved and/or lobbed shape to nuclei. During the second step, through the increasingly deepened invagination nuclei “disrupt” into separate fragments or so that each lobe gives rise to individual micronucleus. Understanding how these nuclear transformations interact with nucleolar components is essential for characterizing the cellular response to severe DNA damage. We anticipate that nucleolar structural alterations induced by  $\gamma$ -irradiation will correlate with the progressive fragmentation of nuclear material, offering novel insights into the interplay between chromatin integrity and

nucleolar stability. In this context we observed two kinds of nuclear cleavage process. If the resulting lobe "engulfs" the nucleolus, nuclear disruption forms the nucleolated micronucleus. In opposite cases, micronuclei became anucleolated. Interestingly, apoptosis-associated changes develop asynchronously in both nucleolated and anucleolated micronuclei. Disruption of the nucleus into individually functioning micronuclei as well as following apoptosis were frequently registered in multi-nucleated cells emerged as a result of UV and  $\gamma$ -irradiation [for example see: 8, 54]. However, according our best knowledge there was no comprehensive explanation of underlying sub-cellular and molecular mechanisms, while our observations can be considered as new and original.

In summary, the study contributes valuable insights into the structural changes in nuclear and nucleolar structure under severe DNA damage, highlighting the significance of NAC in nucleolar organization. The observed similarities between chemical inhibition and  $\gamma$ -irradiation effects emphasize the role of NAC in cellular responses to different stressors. Additionally, nucleolar behavior under  $\gamma$ -irradiation may provide a comparative framework for understanding cellular responses to other forms of genotoxic stress, including oxidative damage and radiation-induced senescence. Given the pivotal role of the nucleolus in cellular stress responses, its alterations may serve as biomarkers for assessing DNA damage severity and predicting cellular fate. The findings of this study have broader implications for cancer biology, as nucleolar disorganization is frequently observed in malignancies characterized by genomic instability.

## CONCLUSION

The methodology employed in this study allows for detailed real-time observation of chromatin and nucleolar behavior in response to DNA damage, providing new insights into nuclear and nucleolar resilience and adaptation. Furthermore, the presence of large-scale chromatin rearrangements following irradiation raises important questions regarding the mechanistic links between nuclear deformation, chromatin dynamics, and nucleolar integrity. Notably, organisms are permanently exposed to physical stressors such as UV-radiation and  $\gamma$ -irradiation, yet the structural consequences of such damage on nucleolar architecture remain underexplored. By characterizing nucleolar responses to  $\gamma$ -irradiation at the molecular and structural levels, this study provides new insights into how nuclear and nucleolar components adapt to DNA damage and contribute to cellular stress responses. Amazingly, the structural consequences of such damage on nucleolar architecture remain underexplored. By characterizing nucleolar responses to  $\gamma$ -irradiation at the molecular and structural levels, this study offers new technical approaches that could facilitate elucidation how nuclear and nucleolar components adapt to DNA damage and contribute to cellular stress responses.

As we have seen our research generated a number of issues, challenging to be explored in first line. For example, among the most appealing topics could be: what is damages degree and what type of breaks undergoing both, relaxed and condensed intra-nucleolar fractions of chromatin, being concealed/"protected" by extremely compact composition of the nucleolus? Obviously, the suitable experimental strategies may deal not only with whole cell nucleoli, but may be amenable to purified nucleoli. In this regard, another interesting question is: whether or not applied 30 Gy  $\gamma$ -irradiation irradiation affect critically template and/or linked transcription machinery, so that isolated nucleoli became transcriptionally unable. Importantly, this issue as well as other related topics are in progress now at SECCZ.

**REFERENCES**

- [1]. Akbari, E., Eui-Jin Park, E-J., Ajit Kumar Singh, A. K., Vinazyak, V., Virk, R. K. A., Wereszczynski, J., Musselman, C. A. (2023) Multiscale genome organization symposium—annual biophysical society meeting. *Biophysical Reviews* 15(3), DOI: 10.1007/s12551-023-01063-8;
- [2]. Frederick, J., Virk, R. K. A., Ye, I. C., Almossalha, L. M., Wodarczyk, G., Van Derway, D., Gonzalez, P. C., Nap, R. J., Agrawal V., Anthony, N. M., Carinato, J., Li, W. S., Dunton, C. L., Medina, K. I., Kakkaramadam, R., Jain, S., Shahabi, S., Ameer, G., Szlafer, I. G., Backman, V. (2024). Leveraging chromatin packing domains to target chemoevasion in vivo. *bioRxiv Preprint*, DOI: 10.1101/2024.11.14.623612;
- [3]. Eid, A., Eshein, A., Li, Y., Virk, R., Van Derway, D., Zhang, D., Taflove, A., Backman, V. (2020) Characterizing chromatin packing scaling in whole nuclei using interferometric microscopy. *Optics Letters*, 45(17): 2-5;
- [4]. Yue Li, Y., Eshein, A., Virk, R., Eid, A., Van Derway, D., Frederick, J., Bleher, R., Szlafer, I. G., Dravid, V., Vadim Backman (2020) Nanoscale Chromatin Imaging and Analysis (nano-ChIA) Platform Bridges 4-D Chromatin Organization with Molecular Function. *Microscopy and Microanalysis*, 26(S2): 1-5;
- [5]. Nishimaki, N., Tsukimoto, M., Kitami, A., Kojima, S. (2012) Autocrine regulation of  $\gamma$ -irradiation-induced DNA damage response via extracellular nucleotides-mediated activation of P2Y6 and P2Y12 receptors. *DNA Repair*: 11: 657-665;
- [6]. Lee, C. H., Wu, S. B., Hong, C. H., Yu, H. S., Wei, Y. H. (2013) Molecular mechanisms of UV-induced apoptosis and its effects on skin residential cells: The Implication in UV based Phototherapy. *Int. J. Mol. Sci.*, 14(3): 6414-6435;
- [7]. Ghorai, A., Bhattacharyya, N. P., Sarma, A., Ghosh, U. (2014) Radiosensitivity and induction of apoptosis by high LET carbon ion beam and low LET gamma radiation: A comparative study. *Scientifica*, 2014: 1-10;
- [8]. Salucci, S., Burattini, S., Batistelli, M., Baldassarri, V., Maltarolo, M. C., Falcieri, E. (2013) Ultraviolet B (UVB) Irradiation-Induced Apoptosis in Various Cell Lineages in Vitro. *Int. J. Mol. Sci.*, 14: 532-546;
- [9]. Juliana, H., Osaki, Espinha, Y. T., Magalhaes, Forti, F. L. (2015) Modulation of RhoA GTPase activity sensitizes human cervix carcinoma cells to  $\gamma$ -radiation by attenuating DNA repair pathways. *Oxidative Medicine and Cellular Longevity*, 2016: 1-11;
- [10]. Zhoo, H., Zhuang, Y., Li, R., Liu, Y., Mei, Z., He, Z., Zhou, F., Zhou, Y. (2018) Effect of different doses of X-ray irradiation on cell apoptosis, cell cycle, DNA damage repair and glycolysis in He-La cells. *Oncology Letters*, 11: 42-54;
- [11]. Azzouz, P., Khan, M. A., Sweerey, N., Palaniar, N. (2018) Two-in one: UV radiation simultaneously induces apoptosis and NETosis. *Cell Death Discovery*, 4: 51-78;
- [12]. Brunner, S., Varga, D., Bozó, R., Polanek, R., Tóké, T., Szabó, E. R., Molnár, R., Gémes, N., Szebeni, G. J., Puskás, J. L., Erdélyi, M., Hideghéty, K. (2021) Analysis of ionizing radiation induced DNA damage by superresolution dSTORM microscopy. *Pathology and Oncology Research*, 27: 160-173;
- [13]. Vickers, E. R. (2022) Human Adipose Stem Cells Exposed to Gamma radiation and inactivity (stasis) show increased cancer markers and DNA damage. A preliminary assessment of a pharmaceutical formulation to reverse these effects and its applications for medical radiotherapy and the space industry. *Journal of Cancer Therapy*, 13: 7-19;
- [14]. Tchelidze, P., Benassarou, A., Kaplan, H., O'Donohue, M. F., Lucas, L., Terryn, C., Rusishvili, L., Mosidze, G., Lalun, N., Ploton, D. (2017) Nucleolar sub-compartments in motion during rRNA synthesis inhibition: contraction of nucleolar condensed chromatin and gathering of fibrillary centers are concomitant. *PLOS one*: 30: 2-37;
- [15]. Busch, H., Smetana, K. (1970) *The Nucleolus*. New York, Academic Press: 1-282;
- [16]. Smetana, K., Busch, H. (1974) The nucleolus and nucleolar DNA. In: Busch H, editor. *The Cell Nucleus*. New York, Academic Press: 73-147;

- [17].Hadjiolov, A. (1985) The Nucleolus and ribosome biogenesis. In: Alfert, M, Beerman W, Goldstein, L, Porter, KR, Site P, editors. Cell Biology Monographs Wien, New York, Springer Verlag: 1-263;
- [18].Thiry, M., Lafontaine D. (2005) Birth of a nucleolus: the evolution of nucleolar compartments. Trends in Cell Biology, 15:194-199;
- [19].Boisvert, F. M., van Koningsbruggen, S. N., Navascues, J., Lamond, A. I. (2007) The multifunctional nucleolus. Nat Rev Mol Cell Biol, 8:574-585;
- [20].Stults, D. M., Killen, M. W., Pierce, H. H., Pierce, A. J. (2008) Genomic architecture and inheritance of human ribosomal RNA gene clusters. Genome Res, 18:13-18;
- [21].Hernandez-Verdun, D., Roussel, P., Thiry, M., Sirri, V., Lafontaine, D. (2010) The Nucleolus: structure/function relationship in RNA metabolism. WIREs RNA, 1:415-431;
- [22].Pederson, T. (2010) The nucleus introduced. Cold Spring Harb Perspect Biol, 10:1-16;
- [23].Olson, M. O. J. (2011) The nucleolus: A nuclear body full of surprises. In: Olson M. O. J. editor. The Nucleolus. Protein Reviews, New-York, Dordrecht, Heidelberg, London: Springer, 15:5-17;
- [24].Baserga, S. J., DiMario, P. J., Duncan, F. E. (2019) Emerging roles for nucleolus 2019. JBC, 295(16): 5535-5537;
- [25].Berus, T., Markiewicz, A., Biecek, P., Orlowska-Heitzman, J., Aalon, A., Romnowska-Dixon, B., Donizi, P. (2020). Clinical significance of nucleoli cytomorphology assessment in patients with uveal melanoma. Anticancer Research, 40 (6): 3505-3512;
- [26].Lafita-Navarro, M. C. Conacci-Sorrell, M. (2022) Nucleolar stress: From development to cancer. Seminars in Cell and Developmental Biology, 136(4): 11- 23;
- [27].Korsholm, L.M., Gál, Z., Bernáldez, B. N., Quevedo, O., Boukoura, S., Lund, CC., Larsen, D. (2020) Recent advances in the nucleolar responses to DNA double-strand breaks. Nucleic Acids Research, 48 (17): 2-12;
- [28].Reynolds, R. C., Montgomery P. 3O., Hughes, B. (1964) Nucleolar “caps” produced by actinomycin D. Cancer Res, 24: 1269-1277;
- [29].Simard, R., Langelier, Y., Mandeville, R., Maestracci, N., Royal, A. (1974) Inhibitors as tools in elucidating the structure and function of the nucleus. In: Busch H, editor. The Cell Nucleus. New York: Academic Press: 447-487;
- [30].Puvion-Dutilleul, F., Mazan, S., Nicoloso, M., Pichard, E., Bachellerie, J. P, Puvion, E. (1992) Alterations of nucleolar ultrastructure and ribosome biogenesis by actinomycin D. Implication for U3 snRNP function. Europ J Cell Biol, 58:149-16;
- [31].Olson, M. (2004) Sensing cellular stress: another new function for the nucleolus? Sci STKE, 10;
- [32].Mayer, C, Grummt, I. (2005) Cellular stress and nucleolar function. Cell Cycle, 4:1036-1038
- [33].Shav-Tal, Y., Blechman, J., Darzacq, X., Montagna, C., Dye, B. T., Patton, J. G. (2005) Dynamic sorting of nuclear components into distinct nucleolar caps during transcriptional inhibition. Mol Biol Cell, 16:2395-2413;
- [34].Tchelidze, P., Kaplan, H., Terryn, C., Lalun, N., Ploton, D., Thiry, M. (2019) Electron Tomography Reveals Changes in Spatial Distribution of UBTF1 and UBTF2 Isoforms within Nucleolar Components during rRNA Synthesis Inhibition. Journal Structural Biology, 208(2): 191-204;
- [35].Michel, J., Nolin, F., Wortham, L., Lalun, N., Tchelidze, P., Banchet, V., Terryn, C., Ploton, D. (2019) Various Nucleolar Stress Inducers Result in Highly Distinct Changes in Water, Dry Mass and Elemental Content in Cancerous Cell Components: Investigation Using Nano-Analytical Approach. Nanoteranostics, 3:179-195;
- [36].Corman, A., Sirozh, O., Lafarga, V., Fernandez-Capetillo, O. (2023) Targeting nucleolus as a therapeutic strategy in human disease. Trends in Biochemical Science, 48(3): 274-287;
- [37].Potapova, T. A., Jay R Unruh, J. R., Conkright-Fincham, J., Banks, C. A. S., Florens, L., David Alan Schneider, D. A., Gerton, J. L. (2023) Distinct states of nucleolar stress induced by anticancer drugs. eLife, 12:1-30;
- [38].Pigg, H. C., Alley K. R., Griffin, C. R., H. Moon, C. H., J. Kraske, S. H., J. DeRose, V. J. (2024) The unique Pt(II)-induced nucleolar stress response and its deviation from DNA damage response pathways. JBC, 300(11): 8567-8581;

- [39].Sellins, K. Cohen, J. (1987) Gene induction by gamma-irradiation leads to DNA fragmentation in lymphocytes. *J. Immunol.*, 139(10): 3199-3206;
- [40].Sudprasert, W., Navasumrit, P., Ruchiravat, M. (2006) Effects of low-dose gamma radiation on DNA damage, chromosomal aberration and expression of repair genes in human blood cells. *Int J Hygiene Env Health*, 209(6): 503-511;
- [41].Dona, M., Ventura, L., Macovei, A., Confalonieri, M., Savio, M., Giovannini, A., Carbonera, D., Balestrazzi, A. (2013) Gamma irradiation with different dose rates induces different DNA damage responses in *Petunia x hybrida* cells, *J Plant Physiol.*, 170(8): 780-787;
- [42].Uttayarat, P., Tangtong, T., Sukapirom, K., Boonsirichai, K. (2015) Gamma irradiation induces DNA double-strand breaks in fibroblasts: a model study for the development of biodosimeter, *J. Phys.: Conf. Ser.*, 611: 012-030;
- [43].Tankovskaia, S. A., Kotb, O. M., Dommes, O. A., Pasten, S. V. (2018) DNA damage induced by gamma-radiation revealed from UV absorption spectroscopy. *J. Phys.: Conf. Ser.*, 1038: 24-26;
- [44].Georkilas, A. (2021) Role of DNA Damage and Repair in Detrimental Effects of Ionizing Radiation. *Radiation*, 1(1): 1-4;
- [45].Afify, A., Ali, H. M., Sayed, R. M. (2024) Estimating the impact of gamma radiation on biochemical aspects and DNA damage by comet assay in *Galleria mellonella* male. *Entomological News*, 131(1): 30-42;
- [46].Mikhailkevich, N., Russ, E., Iordansky, S. (2023) Cellular RNA and DNA sensing pathways are essential for the dose-dependent response of human monocytes to ionizing radiation. *Front. Immunol.*, 14: 123-136;
- [47].Lisowska, H., Deperas-Kaminska, M., Haghdoost, S., Parmryd, I., Wojcik, A. (2010) Radiation-induced DNA damage and repair in human  $\gamma\delta$  and  $\alpha\beta$  T-lymphocytes analysed by the alkaline comet assay. *Genome Integrity*, 1: 8-9;
- [48].Ghorbani, Z., Fardid, R. (2021) Effects of low-dose gamma radiation on expression of apoptotic genes in rat peripheral blood lymphocyte. *Journal of Biomedical Physics and Engineering*, 11(6): 693-700;
- [49].Alghoul, E., Basbous, J., Constantinou, A. (2023) Compartmentalization of the DNA damage response: Mechanisms and functions. *DNA Repair*, 128: 2-12;
- [50].Zhang, X., Wenxin Li, W., Sun, S., Liu, Y. (2024) Advances in the structure and function of the nucleolar protein fibrillarin. *Front. Cell Dev. Biol.*, 12: 14-24;
- [51].Nadaraia, L., Okuneva, O., Gogebashvili, M., Ivanishvili, N., Tchelidze, P. (2023) Nucleolar dynamics: reorganization of nucleolus-associated condensed chromatin under DNA damage induced by different doses of  $\gamma$ -irradiation. *Journal of Radiology and Radiation Safety*, 4(5): 18-36;
- [52].Zatsepina OV, Voit R, Grummt I, Spring H, Semenov MV, Trendelenburg M. The RNA polymerase I specific transcription factor UBF is associated with transcriptionally active and inactive ribosomal genes. *Chromosoma* 1993, 102:599-611;
- [53].Mais C, Wright JE, Prieto JL, Raggett SL, McStay B. UBF-binding site arrays form pseudo-NORs and sequester the RNA polymerase I transcription machinery. *Genes Dev* 2005, 19:1-15;
- [54].Braten, M., Banreed, H., Berg, K., Moan, J. (2000) Induction of multinucleated cells caused by UVA exposure in different stages of the cell cycle. *J Photochem Photobiol B: Biology*, 71(5): 620-626;